Acousto-optic control of speckle contrast in multimode fibers with a cylindrical piezoelectric transducer oscillating in the radial direction

Woosung Ha,[1] Sejin Lee,[1] Yongmin Jung,[2] Jun Ki Kim,[3] and Kyunghwan Oh[1,*]

[1]*Institute of Physics and Applied Physics, Yonsei University, 262 Seongsanno, Seodaemun-gu, Seoul 120-749, Korea*
[2]*Optoelectronics Research Centre, University of Southampton, Southampton, SO17 1BJ, UK*
[3]*Fraunhofer Institute for Applied Optics and Precision Engineering, Albert-Einstein St. 7, 07745 Jena, Germany*
**koh@yonsei.ac.kr*

Abstract: We report efficient acousto-optic control of speckle contrast at the output of multimode fibers (MMFs) using a cylindrical piezoelectric transducer (PZT) vibrating in the radial direction. With appropriate packaging of an MMF around the PZT, periodic stretching and subsequent intensity modulation were achieved over the wound fiber to result in time-averaged smoothing of the output within a short time. It was experimentally confirmed that light passed through the vibrating PZT-fiber assembly maintains the virtually partial coherence irrespective of the guide length and power splitting. Real-time vibration-off/on movies were presented, and their single-frame excerpts were analyzed.

OCIS codes: (030.6140) Speckle; (060.2310) Fiber optics; (060.2350) Fiber optics imaging; (230.1040) Acousto-optical devices.

References and links

1. J. W. Goodman, *Speckle Phenomena in Optics: Theory and Applications* (Roberts and Company, Englewood, CO, 2006).
2. T. Iwai, and T. Asakura, "Speckle reduction in coherent information processing," Proc. IEEE **84**(5), 765–781 (1996).
3. H. Ambar, Y. Aoki, N. Takai, and T. Asakura, "Mechanism of speckle reduction in laser-microscope images using a rotating optical fiber," Appl. Phys. B **38**(1), 71–78 (1985).
4. P. J. Kajenski, P. L. Fuhr, and D. R. Huston, "Mode coupling and phase modulation in vibrating waveguides," J. Lightwave Technol. **10**(9), 1297–1301 (1992).
5. K.-I. Sato, and K. Asatani, "Speckle noise reduction in fiber optic analog video transmission using semiconductor laser diodes," IEEE Trans. Commun. **29**(7), 1017–1024 (1981).
6. Y. Jeong, D. Lee, J. W. Lee, and K. Oh, "Fiber-optic color synthesizer," Opt. Lett. **31**(14), 2112–2114 (2006).
7. J. K. Kim, H. R. Kim, A. Tünnermann, and K. Oh, "Synthesis of pure white color and its equal power, equal chromatic splitting through a novel 3x3 fiber optic visible multiplexer," Opt. Express **16**(22), 17319–17328 (2008), http://www.opticsinfobase.org/oe/abstract.cfm?uri=oe-16-22-17319.
8. A. P. Povilus, S. E. Olson, R. R. Mhaskar, B.-K. Teo, J. R. Guest, and G. Raithel, "Time averaging of multimode optical fiber output for a magneto-optical trap," J. Opt. Soc. Am. B **22**(2), 311–314 (2005).
9. Y. B. Yeo, H. J. Jeong, Y. W. Koh, and B. Y. Kim, "All fiber-optic polarization scrambler," presented at the Second Optoelectronics and Communications Conference, Seoul, Korea, 8–11 July 1997.
10. O. I. Kotov, A. V. Khlybov, L. B. Liokumovich, S. I. Markov, A. V. Medvedev, V. A. Rukavishnikov, A. I. Borovkov, and D. V. Shevchenko, "Polarization modulation of light in an optical waveguide under lateral compression," Tech. Phys. **51**(11), 1494–1499 (2006).
11. J. O. Kim, K. K. Hwang, and H. G. Jeong, "Radial vibration characteristics of piezoelectric cylindrical transducers," J. Sound Vibrat. **276**(3-5), 1135–1144 (2004).
12. B. Daino, G. de Marchis, and S. Piazzolla, "Analysis and measurement of modal noise in an optical fibre," Electron. Lett. **15**(23), 755–756 (1979).
13. E. G. Rawson, J. W. Goodman, and R. E. Norton, "Analysis and measurement of the modal-noise probability distribution for a step-index optical fiber," Opt. Lett. **5**(8), 357–358 (1980).
14. D. U. Kim, S. C. Bae, J. Kim, T.-Y. Kim, C.-S. Park, and K. Oh, "Hard polymer cladding fiber (HPCF) links for high-speed short reach 1×4 passive optical network (PON) based on all-HPCF compatible fused taper power splitter," IEEE Photon. Technol. Lett. **17**(11), 2355–2357 (2005).

#112838 - $15.00 USD Received 15 Jun 2009; revised 12 Sep 2009; accepted 14 Sep 2009; published 16 Sep 2009

1. Introduction

Laser power delivery over optical fibers provides significant advantages such as less exposed optical access, flexible alignment, and safety. Single-mode fibers (SMFs) have been widely used as their output provides a well-defined Gaussian-like spatial mode. However, due to the small core and subsequent optical nonlinearity, SMFs suffer from low coupling efficiencies, optical damage, and pointing instabilities. Therefore, in recent high-power laser delivery, SMFs are being replaced by multimode fibers (MMFs) that are equipped with a large core diameter, high numerical aperture (NA), and low nonlinearity. Even though the problems in SMFs can be resolved by the use of MMFs, peculiar granularities appear at MMF outputs when a coherent light is guided, which results in degradation of the quality of the spatial mode. This random intensity distribution is referred to as a speckle pattern and is attributed to the interference between the guided modes traveling within the fiber [1].

To reduce the speckle contrast, various techniques have been developed, and their principles can be simply summarized by controlling the coherence of the illuminating light and then averaging several uncorrelated speckle images in space and time [2]. To circumvent a high-cost and complex structure system, vibration techniques have been introduced that utilize both mode coupling and phase modulation [3,4]. However, to practically reduce the speckle contrast in such cases, longer exposure time and post-processing were required for effective ensemble averaging of uncorrelated patterns on an irradiance basis. These restrictions did not provide fundamental solutions to the applications requiring constant illumination and caused intensity saturation in the detecting system that adopted a charge-coupled device (CCD).

Coherent light delivery over MMFs has continuously gained attention and interest for many imaging applications such as direct image delivery [2], analog video signal transmission [5], and fiber-based color synthesis [6,7], and has been accompanied by a demand for efficient and fast control of the speckle contrast. The acousto-optic modulation technique based on a piezoelectric transducer (PZT) could provide a common solution platform for MMF laser delivery applications. Recently, Povilus et al. briefly reported a speckle-modulation technique using a cylindrical PZT to stabilize magneto-optical atom trapping [8]. Although the technique enabled time-averaged smoothing within a short time without post-processing, speckle control in MMFs has not been fully studied. Furthermore, in contrast to the elasto-optic polarization modulation in an SMF under lateral compression [9,10], detailed analyses of various types of MMFs under radial stress by the PZT have been very scarce, especially in terms of parametric and statistical studies.

In this paper, we report systematic and parametric analysis of the spatial coherence control using the cylindrical PZT for two widely used types of MMFs, a 50-μm-core graded-index MMF (GI-MMF) and a 200-μm-core step-index hard polymer-clad fiber (HPCF), for the first time, to the best knowledge of the authors. Experimental comparison of the radial vibration response for the GI-MMF and the HPCF was made using the common PZT platform. In the GI-MMF both core and cladding are silica glass, while in the HPCF the cladding is polymer. Phase modulation and mode coupling in the glass cladding and polymer cladding were compared, which could have a high potential to provide an optimal waveguide structure design for the coherence control. Comparative statistical analyses are also reported to characterize the acousto-optic interaction with the GI-MMF and the HPCF.

2. Theory

When an optical waveguide is externally disturbed, the distribution of light in the output pattern is modulated due to phase modulation and mode coupling of the guided modes [4]. Various analyses have been performed for phase modulation [1,4,8], and the main conclusion for effective smoothing of the spatial modes was that the relative carrier phase should be

#112838 - $15.00 USD Received 15 Jun 2009; revised 12 Sep 2009; accepted 14 Sep 2009; published 16 Sep 2009

varied by more than 2π radian on a time scale faster than the response time of the detecting system.

The change in the power of the mth mode by mode coupling can be described as

$$\Delta P_m = \sum_{n=1}^{N} h_{mn}(P_m - P_n), \tag{1}$$

where h_{mn} is the coupling coefficient between the guided modes of m and n, P_m is the initial power in mode m, and N is the total number of bound modes. If h_{mn} becomes larger in a random manner by external perturbations, the average power of the speckle regions increases [4] and the contrast decreases, which results in a more uniform fiber output. Therefore, we derive the relation between h_{mn} and experimental parameters to find optimal conditions of homogenization, but thorough calculation of Eq. (1) for all the available modes in the MMFs would not be evaluated because it is beyond the scope of this study. If the fiber deformation function $f(z)$ is known over a length of fiber L, the power coupling coefficient between modes m and n over this distance can be expressed as

$$h_{mn} = K_{mn}^2 F_{mn}^2, \tag{2}$$

where K_{mn} is a constant depending on the fiber structure, and

$$F_{mn} = \int_{-L/2}^{L/2} f(z) e^{i(\beta_m - \beta_n)z} dz, \tag{3}$$

where β_m and β_n are the propagation constants of modes m and n, respectively.

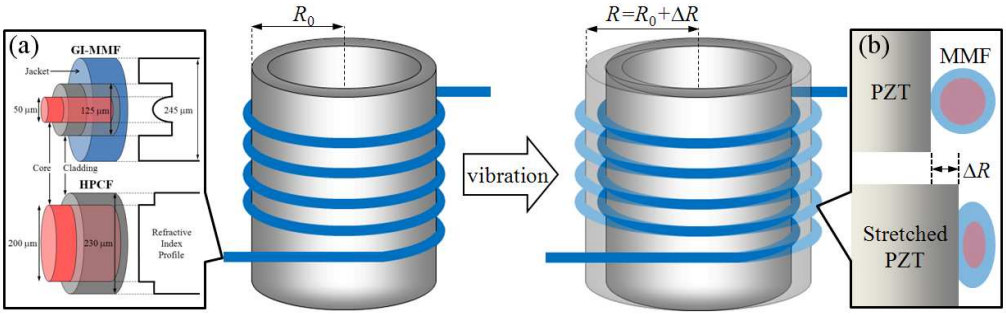

Fig. 1. Schematic diagram of the PZT-fiber assembly. The inset (a) shows the dimensions of the MMFs used in our experiments and their refractive index profiles. The inset (b) shows exaggerated cross-sectional views of the assembly before (upper) and after (lower) stretching.

The schematic of the PZT-fiber assembly in our experiments is shown in Fig. 1, and in this case, the function F_{mn} can be modified as

$$F_{mn} = n_t \int_{-\pi R_0}^{\pi R_0} f_1 e^{i(\beta_m - \beta_n)z} dz, \tag{4}$$

where n_t is the total number of coils turned around the mandrel, f_1 is the fiber deformation function for the length of a single turn, and R_0 is the initial outer radius of the PZT. Therefore, f_1 could be set as $f_1 = f_c(z) + 2\pi\Delta R$, where $f_c(z)$ is the fiber deformation function for the bending of the circular shape and ΔR is the increment of the PZT radius. Note that $2\pi\Delta R$ of f_1 is independent of the propagation position because the overall part of the fiber attached to the PZT would be stretched simultaneously. If we drive the PZT with sinusoidal voltage $V = V_0 \sin(\omega_v t)$ where V_0 is amplitude, ω_v is frequency, and t is time, then the radius of the PZT will have an oscillating increment as

$$\Delta R = \delta_R(\omega_v) V_0 \sin(\omega_v t), \tag{5}$$

#112838 - $15.00 USD Received 15 Jun 2009; revised 12 Sep 2009; accepted 14 Sep 2009; published 16 Sep 2009

where $\delta_R(\omega_v)$ is the amplitude per unit voltage for ω_v [11]. Because we are interested only in a time-varying term, time-independent $f_c(z)$ of f_1 will be not considered in the following steps. Then, Eq. (4) would be further changed as

$$\begin{aligned}\Delta F_{mn}(t) &= 2\pi\delta_R(\omega_v) n_t V_0 \sin(\omega_v t)\int_{-\pi R_0}^{\pi R_0} e^{i(\beta_m-\beta_n)z} dz \\ &= 4\pi^2\delta_R(\omega_v) n_t R_0 V_0 \sin(\omega_v t)\mathrm{sinc}\left(R_0(\beta_n-\beta_m)\right),\end{aligned} \tag{6}$$

where the sinc function is normalized. Substitution of this result into Eq. (2) yields that

$$\Delta h_{mn}(t) = C_{mn}(R_0)\left[K_{mn}\delta_R(\omega_v)V_0\right]^2 n_t^2 \sin^2(\omega_v t), \tag{7}$$

where $C_{mn}(R_0) = 16\pi^4 R_0^2 \mathrm{sinc}^2(R_0(\beta_n - \beta_m))$.

From Eq. (7), it is noted that the power fluctuation is highly affected by key parameters such as the fiber structure factor K_{mn}, the material and electrical properties of the PZT $\delta_R(\omega_v)$, the number of coils n_t, and the amplitude of driven voltage V_0. Mode coupling constant $C_{mn}(R_0)$ is proportional to the sinc function in terms of the propagation constant difference ($\beta_n - \beta_m$), which gets a small value among high-order modes. Therefore, mixing of the guided lights will be more effective among the high-order modes than among low-order modes because the sinc-function properties peaked at zero. Because R_0 is related to both $C_{mn}(R_0)$ and $\delta_R(\omega_v)$, R_0 needs to be optimized to maximize the mode mixing efficiency.

By these mode coupling and phase modulation processes, the light passed through the PZT-fiber assembly can be modified to have the virtually partial coherence [2]. The term "virtually" means that the degeneration of spatial coherence in the source can be realized. As we will discuss at the end of section 4, the virtually partial coherence in the proposed device was successfully maintained irrespective of the guide length and the splitting, which can be directly utilized in the imaging processing mentioned in the introduction.

3. Device structure and optimal operation frequency

The GI-MMF (LS Cable) used in these experiments had a 50-μm GeO_2-P_2O_5 co-doped silica core, 125-μm silica cladding, and acrylate polymer jacket of a 250-μm diameter with an NA of 0.203. The HPCF (SSCP) was composed of a 200-μm pure silica core along with 15-μm thick low-index polymer cladding. The waveguide had the step-index structure with core and cladding refractive indices of 1.45 and 1.40, respectively. The typical NA of the HPCF ranged from 0.37 to 0.48. It is noted that the GI-MMF has a glass core and glass cladding, while the HPCF has a glass core and polymer cladding. Due to the larger core and the higher refractive index difference, the HPCF holds more guiding modes than the GI-MMF. The dimensions and the refractive-index profiles of the GI-MMF and the HPCF are shown in the inset (a) of Fig. 1.

The cylindrical lead-zirconate-titanate PZT used in the experiments was EC-64 produced by EDO Corporation. The PZT had an outer diameter of 38 mm, 2-mm thickness, and 38-mm height. Around the cylindrical PZT, 5-m-long MMFs were tightly coiled 20 times in circles and then bonded with epoxy. Note that the number of coils n_t should be kept no more than 20 so that PZT's oscillation could play a major role by dominating time-independent mode coupling. When a radio-frequency (RF) sinusoidal driving signal was applied at the PZT, the fiber was vibrated by the radially expanding PZT as well as local bending to result in phase modulation and mode coupling.

A highly coherent He-Ne laser source (wavelength λ = 632.8 nm) was coupled to the MMFs and transmitted through the PZT-fiber assembly. The output was directly imaged by a CCD camera (Toshiba IK-642F) with an objective lens of × 60 (NA 0.85) for the GI-MMF and × 20 (NA 0.40) for the HPCF. The CCD camera had the exposure time of 1/30 seconds and the resolution of 640 × 480 pixels. For near-field measurements the objective lenses were

#112838 - $15.00 USD Received 15 Jun 2009; revised 12 Sep 2009; accepted 14 Sep 2009; published 16 Sep 2009

focused on the fiber output surfaces, while for far-field measurements they were moved backward by 100 μm from the GI-MMF and 300 μm from the HPCF. The power of the laser source was suitably scaled to prevent the saturation of the CCD. The RF modulation frequency was controlled by a function generator (Agilent 33120A) with an amplifier. Throughout the entire experimental process, external vibrations other than PZT vibration were minimized on a floated optical table because a beam pattern is very sensitive to the mechanical perturbation along the optical path. Actual movies of vibration-off/on states were taken by the CCD camera, and quantitative analysis was performed by counting the number of pixels for digitally 256-level intensities in selected areas with the image-processing software National Instrument IMAQ Vision Builder.

For the proposed assembly made of the GI-MMF and the HPCF, we investigated the modulation-frequency dependence on the speckle reduction. A widely used physical measurand for the speckle pattern is the contrast of the intensity [1] defined as

$$C = \frac{\sqrt{\langle I^2 \rangle - \langle I \rangle^2}}{\langle I \rangle} = \frac{\sigma_I}{\langle I \rangle}, \tag{8}$$

where I and $\langle I \rangle$ are the intensity and its mean value, respectively, and σ_I is the standard deviation of I within the speckle pattern. If ΔR increases, the modulation effect is increased, and reduced speckle contrast is expected. Therefore, the time-averaged smoothing effect will maximize the reduction of speckle contrast at the natural frequencies of the PZT. The fundamental natural frequency ω_0 can be estimated according to the reference [11], and in our experiments ω_0 was predicted to be near 24 kHz.

The driving frequency and voltage of the PZT were scanned in the range from 0 to 40 kHz and from 0 to 20 V peak to peak (Vpp), respectively. The optimal results in coherence control were obtained only in the vicinity of 24 kHz, which were related with the natural frequency of the cylindrical PZT [11]. The voltage response showed the linear increase in the coherence control, which showed saturation above 10 Vpp in the case of the HPCF. By taking the fiber output images for every frequency increment of 10 Hz, we obtained a total of 401 images. For a certain circular area of fiber's output, the software analyzed the images in terms of I and calculated $\langle I \rangle$ and σ_I. For the GI-MMF, we investigated 18,980 and 26,976 pixels for the near and far fields, respectively. For the HPCF that has a larger core than the GI-MMF, we investigated 25,836 and 33,160 pixels for the near and far fields, respectively. Dimensions and locations of the analyzed regions would be introduced in the next section. We carefully maintained the analyzed regions for each image to be overlaid in the exactly same spatial region. The contrast C as defined in Eq. (8) was calculated for every PZT-driving frequency, and the results are summarized in Fig. 2.

For a fixed modulation voltage of 10 Vpp, resonant characteristics were clearly observed for the GI-MMF with distinct minima for both near and far field images. Although the minima were equal to the peak ω_v of the GI-MMF, the HPCF shows two extreme cases; the average C values at the near field are significantly low, but the far-field pattern is seldom affected by ω_v holding high C. The latter can be solved by y-axis calibration or by increasing the signal voltage. The former can be contributed to the unusual HPCF structure. As one can see in Fig. 1, the thin polymer cladding of the HPCF will create a much larger acousto-optic effect than the GI-MMF, and will raise the modulation efficiency, namely high K_{mn}. It results in strong mode coupling even in the absence of any vibration as in Eq. (2), and a measured C at its vibration-off state was much lower than the others due to the bending effect. Actually, the speckle-reducing effect could be easily saturated by weak oscillation, which was confirmed by comparison of the C values for various V_0. Considering all the cases, it would be reasonable to take ω_0 = 24.16 kHz for the lowest C. The remaining parts of this paper will refer to the vibration-on state as $\omega_v = \omega_0$.

#112838 - $15.00 USD Received 15 Jun 2009; revised 12 Sep 2009; accepted 14 Sep 2009; published 16 Sep 2009

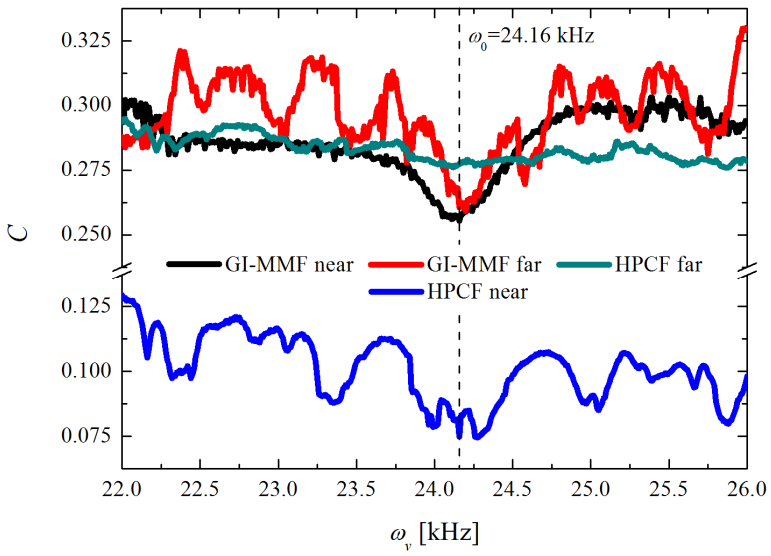

Fig. 2. The contrast of the intensity as a function of the driven frequency for 10 Vpp. stretching.

4. Experimental results

To visually confirm the effect of acousto-optic modulation through the proposed assembly, we captured images of the output from the test fibers for the vibration-off/on states at the driving voltage of 40 Vpp. Here the modulation frequency was maintained at ω_0 = 24.16 kHz, and the results are summarized in Fig. 3. Note that the distances between the observation points of the near and far fields were 100 μm for the GI-MMF and 300 μm for the HPCF. Speckle patterns emerged from the MMFs are gradually transformed by Fresnel and Fraunhofer diffractions, which results in higher contrasts in the far-field observation than in the near field. Without vibration, very conspicuous speckle noises with high contrast were observed in both GI-MMF and HPCF. The average speckle sizes in the near- and far-field measurements were 12 pixels and 21 pixels in both GI-MMF and HPCF. The near- and far-field diameters for the fiber outputs in the number of pixels were also listed in Table 1, which corresponds to the green circles in Fig. 3. When the acoustic modulation was turned on, contrast values for the areas inside the green circles were significantly reduced by mode coupling and phase modulation. In the GI-MMF, the contrast decreased from 0.184 to 0.150, equivalent to an 18.5% reduction for the near field, and from 0.201 to 0.180, a 10.4% reduction for the far field. In the HPCF, the contrast decreased from 0.124 to 0.088, a 29.0% reduction for the near field, and from 0.221 to 0.192, corresponding to a 13.1% reduction for the far field. Additional speckle contrast incurred by Fresnel and Fraunhofer diffractions is inherently unavoidable, and therefore mode coupling and phase modulation induced by the PZT had less reduction efficiency for the far-field patterns. It is noted that the reduction of the speckle contrast in the GI-MMF in these experiments is better than in prior results [2,3]. It is also noteworthy that, for the same acoustic modulation, the HPCF showed better constant reduction than the GI-MMF. This result is attributed to the polymer cladding in the HPCF, where the evanescent waves of the guided modes are directly exposed to acousto-optically driven deformations directly contributing to mode coupling and phase modulation. In the GI-MMF, however, the modes are guided by the glass core and glass cladding, which are protected by acrylate jacketing. This jacketing serves as a sort of damper for the acousto-optic deformation to decrease the contrast reduction efficiency. We included Media 1 to clearly show the distinct differences between the modulation off and on states. The bottom of Fig. 3 shows the digitally magnified images by 20 times for the central region of each vibration-on

#112838 - $15.00 USD Received 15 Jun 2009; revised 12 Sep 2009; accepted 14 Sep 2009; published 16 Sep 2009

state by a commercial image viewing program, where periodic noise patterns were observed. However, these were not real speckles out of optical fibers but the structure of the CCD camera used in the experiments caused by the edge effect. The inherent noises from the CCD were measured using incoherent white light at a non-saturating power level. Speckle-free light from the fibers was measured by the CCD camera to find the contrast of 0.030 for a circular region of 25,836 pixels allowing fluctuating errors of ± 0.65 in the $I/\langle I \rangle$ profiles.

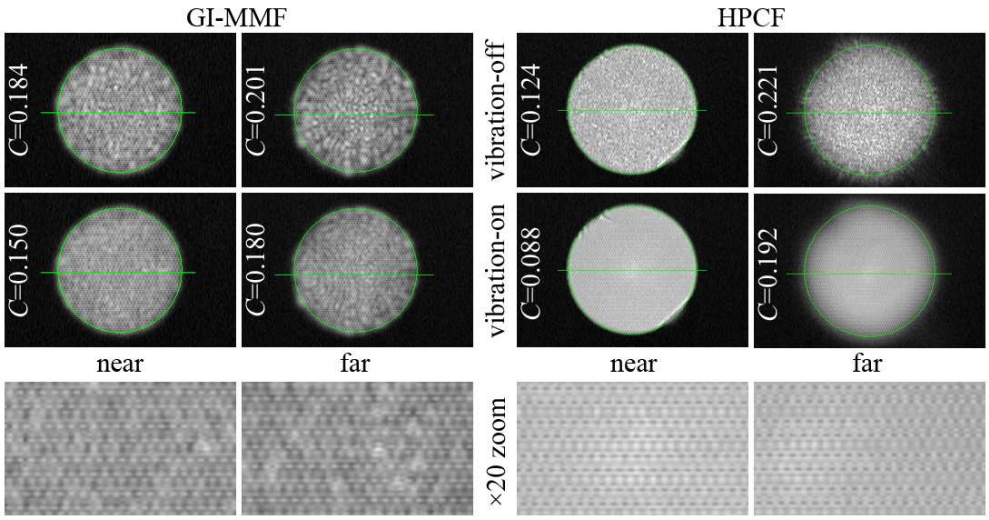

Fig. 3. Single-frame excerpts from a video recording of fiber output at the near and far fields of the GI-MMF and the HPCF through the CCD camera for the vibration-off/on states with 40 Vpp (Media 1). The bottom images show 20-time magnifications of the central regions for each vibration-on state.

Table 1. The average speckle size and the fiber output diameters in the number of pixels

	GI-MMF		HPCF	
	Near	Far	Near	Far
Speckle	12	21	12	21
Output diameter	142	176	194	218

For the CCD images of the direct outputs of optical fibers in Fig. 3, we further analyzed the line profiles across the centers as indicated in the green horizontal lines marked at the fiber images. The line profiles are summarized in Fig. 4. In the figure, we used the relative intensity $I/\langle I \rangle$ instead of I for statistical analysis as in the reference [1], which is widely used in speckle analysis [12,13]. This relative intensity analysis is also reasonable because the input power values were set differently for each case to avoid CCD saturation. The mean value of intensity was obtained from the region within the green circles in Fig. 3, the exactly same location used to obtain the results in Fig. 2. The fluctuations in the relative intensity were also significantly reduced to provide a stabilized profile, especially for the HPCF. The output of the HPCF at the near field shows an almost flat-top distribution, and the relative intensity values were kept constant as unity. Fine fluctuations in that profile can be negligible because the errors stem from the periodic noises as mentioned. The far-field images also showed stable line profiles under acousto-optic modulation, but the output pattern was no longer a flat-top distribution.

#112838 - $15.00 USD Received 15 Jun 2009; revised 12 Sep 2009; accepted 14 Sep 2009; published 16 Sep 2009

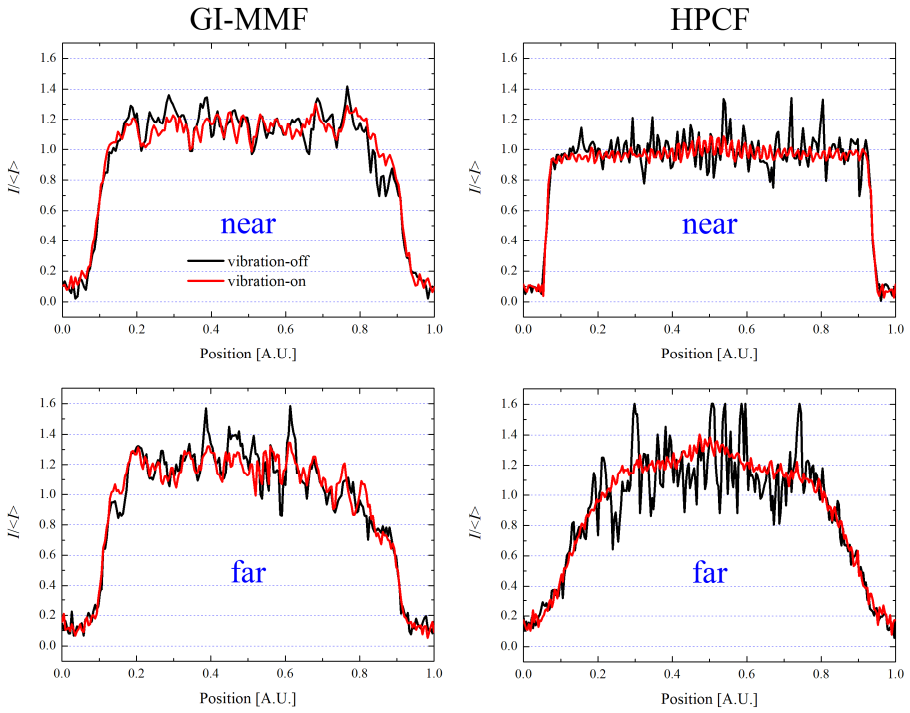

Fig. 4. Line profiles for near and far fields of the GI-MMF and the HPCF marked as green horizontal lines in Fig. 3. Chaotic lines were significantly relieved at the illuminated region.

The unconstrained probability density function (PDF) of a speckle pattern at the output of MMFs is known to be given by a gamma density function [1],

$$p\left(I/\langle I\rangle\right)=\frac{N^N\left(I/\langle I\rangle\right)^{N-1}\exp\left[-N\left(I/\langle I\rangle\right)\right]}{\langle I\rangle\Gamma(N)}, \tag{9}$$

where N is the total number of correlation cells across the output and Γ is the gamma function. The PDFs have been reported for a GI-MMF and a step-index MMF [12,13]. However, this statistics are valid only for the case of sufficient ensemble averaging, and instant behavior would contain fluctuations owing to the CCD noises. The PDFs for the GI-MMF and the HPCF were analyzed, and the comparison between the vibration-off/on states is plotted in Fig. 5. The unit of the PDF in our case is the number of the pixels for the selected area, which is given as green circles in Fig. 3. For the GI-MMF, the overall shape follows the gamma density function, and if vibration is applied, the distribution becomes narrower with a decrease in the full width at half maximum (FWHM) and an increase in the peak value. The quasi-symmetric shape about the axis of $I/\langle I\rangle = 1$ was found and the change in the distribution by the vibration was less prominent in the far-field images of the GI-MMF. In the case of the HPCF, the result was very different from that of the GI-MMF. The most remarkable feature during PZT's oscillation was the highly asymmetric distribution in the PDF. Furthermore, in comparison to the case of the vibration-off state, the PDF distribution of the vibration-on state did not follow the conventional gamma density function and was affected by the tightness of coiling of HPCF over the PZT cylinder. This peculiar behavior in the vibrating HPCF has not been reported to our knowledge and attributed to direct modification of the HPCF structure by mechanical perturbation from PZT's oscillation. In contrast to the GI-MMF, the external mechanical perturbations directly alter the cladding boundary of the HPCF, which makes the HPCF no longer a cylindrically symmetric

#112838 - $15.00 USD Received 15 Jun 2009; revised 12 Sep 2009; accepted 14 Sep 2009; published 16 Sep 2009

waveguide. Therefore, in the HPCF, the guided modes themselves are affected by the non-circular-cladding optical fiber. As a supporting evidence of this direct cladding alteration in the HPCF, we found that the PDFs of the HPCF were influenced by fiber-winding tension over the PZT. As we vary the tension from tens of grams to several hundred grams for the HPCF winding, the PDF was indeed changed while the GI-MMF did not result in significant variations for the same range of tension. Detailed theoretical analyses for modification of the waveguide structure in the HPCF are beyond the scope of this study, and remains as a future work pursued by the authors.

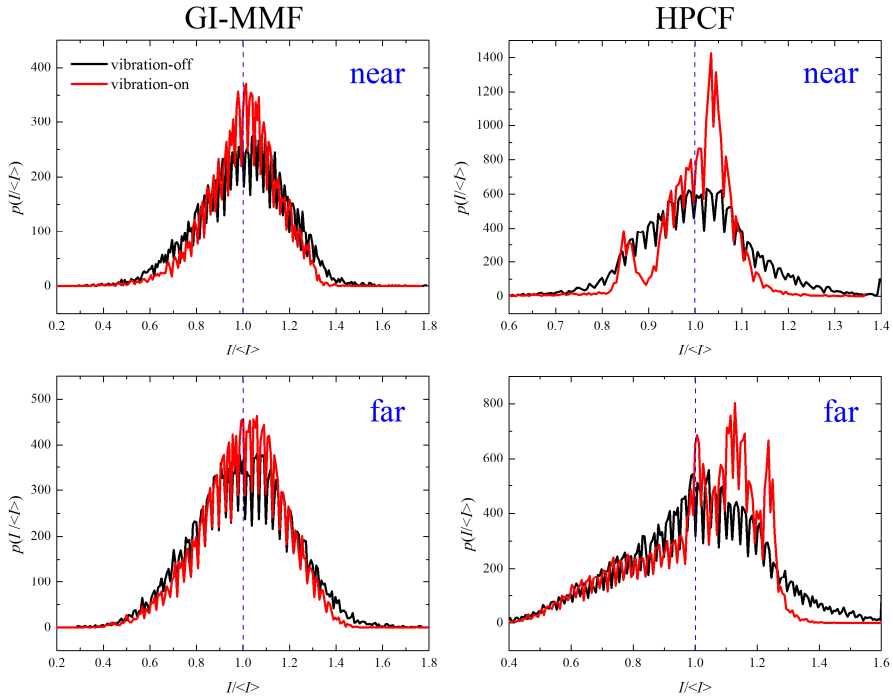

Fig. 5. Experimentally obtained PDFs as a function of relative intensity.

For the proposed assembly, we tested how the virtually partial coherence would be maintained in terms of waveguide length and optical power splitting using a long length test fiber and a 1 × 3 splitter, respectively. The light source through the PZT-HPCF assembly was again focused into a separate 100-meter-long HPCF segment by using a × 20 objective (NA 0.40). The modulation conditions were the same as the previous experiments. The output from the 100-m HPCF was measured, and the results are shown in Fig. 6. Without acousto-optic modulation, the contrast in the area inside the green circle slightly increased to C = 0.135 in comparison to direct output from the assembly, and decreased to C = 0.088 when the modulation was turned on. The line profile was also close to the flat-top distribution, and the PDF still showed asymmetric shape with an increase in bright spots.

We also investigated how the virtually partial coherence would behave under a 1 × 3 HPCF power splitter, and the experimental setup is schematically shown in Fig. 7. The splitter was made by conventional fused tapering technique based on the micro-flame brushing technique [14]. The light source through the PZT-HPCF assembly was again focused into the input port of the splitter using a × 20 objective (NA 0.40). Three output-port images were simultaneously focused into the CCD, and the results are shown in Fig. 7. Similar to the direct output of the assembly, contrast values of the area inside the green circles decreased when the modulation was turned on. The output quality improvement was almost the same, and this can be quantitatively confirmed by obtaining contrast values for each case. We repeated the same

#112838 - $15.00 USD Received 15 Jun 2009; revised 12 Sep 2009; accepted 14 Sep 2009; published 16 Sep 2009

experiment for a 60 × 60 plastic optical fiber coupler to confirm the same results, and confirmed that the virtually partial coherence in the proposed assembly was maintained through a power-splitting device as well as a separate long-length fiber. Reduction of speckle contrast over the long length of a fiber can find direct applications in imaging processing by replacing bulk optic paths with compact and flexible optical fibers. Furthermore, power splitting could allow multiple processing heads of higher efficiency.

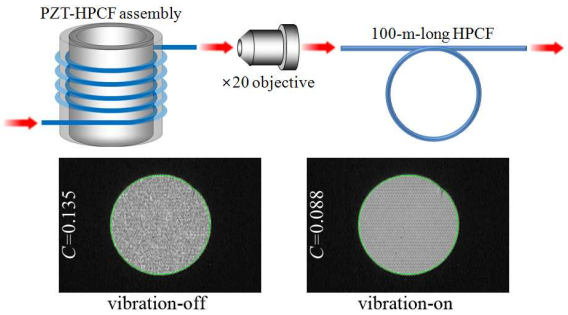

Fig. 6. Fiber output images of the 100-m-long HPCF for the vibration-off/on state.

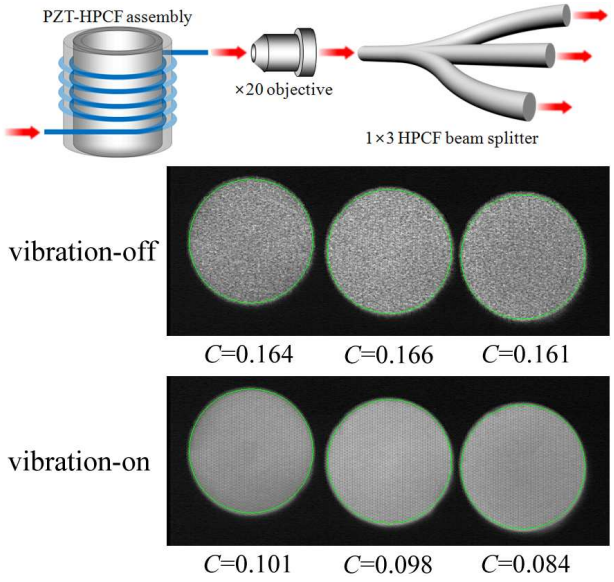

Fig. 7. Schematic diagram of the 1 × 3 HPCF beam multiplexer and their vibration-off/on images at three output ports.

5. Conclusion

In conclusion, we experimentally studied the effective speckle noise reduction in a 50-μm-core GI-MMF and a 200-μm-core HPCF using a cylindrical PZT, where the test fibers were wound over the PZT driven oscillating in the radial direction by the RF wave. Dynamic modulation in the fibers produced a time-averaged smoothing effect in the output field distribution within a very short time, which can obviate further post-processing ensemble averaging. We calculated the speckle contrast after taking a single frame of both MMFs for the vibration-off/on states and an image analyzing software. The effect was maximized at the fundamental natural frequency of the PZT, around 24.16 kHz, and was influenced by their intrinsic fiber parameter. We achieved an almost flat-top output profile with the HPCF, and this enabled us to find the ample potential of the beam homogenizer. Furthermore, the proposed method can be developed as an integrated circuit owing to its considerably reduced

#112838 - $15.00 USD Received 15 Jun 2009; revised 12 Sep 2009; accepted 14 Sep 2009; published 16 Sep 2009

mechanical size of operation. Because time-averaged smoothing is more effective for larger oscillation of the PZT due to acousto-optic modulation, the contrast reduction and the beam quality will be surely improved by adopting a high-performance piezoelectric material or a signal amplifier. It was also experimentally confirmed that the virtually partial coherence through the assembly is maintained irrespective of long-range delivery and beam splitting. We expect that the proposed speckle-reducing technology would extend a choice of optical sources to coherent laser in many imaging applications.

Acknowledgments

This work was supported in part by the NRF (Grant Nos. ROA-2008-000-20054-0, R15-2004-024-00000-0, 2008-8-1893 (EC-FP7/2007-2013 GOSPEL project 219299), and 2009-8-1339 with the Brain Korea 21 Project) and in part by the ITEP (Grant Nos. 2008-8-1195 and 2008-8-1891).

#112838 - $15.00 USD Received 15 Jun 2009; revised 12 Sep 2009; accepted 14 Sep 2009; published 16 Sep 2009